J. E. Castellini, C. A. Faulkner, W. Zuo, D. M. Lorenzetti, and M. D. Sohn 2022. "Assessing the Use of Portable Air Cleaners for Reducing Exposure to Airborne Diseases in a Conference Room with Thermal Stratification." Buildings and Environment, 207 (B), pp. 108441, doi: https://doi.org/10.1016/j.buildenv.2021.108441.

Assessing the Use of Portable Air Cleaners for Reducing Exposure to Airborne Diseases in a Conference Room with Thermal Stratification

John E. Castellini Jr.[a], Cary A. Faulkner[a], Wangda Zuo[a,b,c], David M. Lorenzetti[d], Michael D. Sohn[d]

[a]*Department of Mechanical Engineering, University of Colorado Boulder, UCB 427, Boulder, 80309, CO, U.S.A.*
[b]*Department of Civil, Environmental and Architectural Engineering, University of Colorado Boulder, UCB 428, Boulder, 80309, CO, U.S.A.*
[c]*National Renewable Energy National Laboratory, Golden, 80401, CO, U.S.A.*
[d]*Energy Analysis and Environmental Impacts Division, Lawrence Berkeley National Laboratory, 1 Cyclotron Road, Berkeley, 94720, CA, U.S.A.*

Abstract

The COVID-19 pandemic has highlighted the need for strategies that mitigate the risk of aerosol disease transmission in indoor environments with different ventilation strategies. It is necessary for building operators to be able to estimate and compare the relative impacts of different mitigation strategies to determine suitable strategies for a particular situation. Using a validated CFD model, this study simulates the dispersion of exhaled contaminants in a thermally stratified conference room with overhead heating. The impacts of portable air-cleaners (PACs) on the room airflow and contaminant distribution were evaluated for different PAC locations and flow rates, as well as for different room setups (socially distanced or fully occupied). To obtain a holistic view of a strategy's impacts under different release scenarios, we simultaneously model the steady-state distribution of aerosolized virus contaminants from eight distinct sources in 18 cases for a total of 144 release scenarios. The simulations show that the location of the source, the PAC settings, and the room set-up can impact the average exposure and PAC effectiveness. For this studied case, the PACs reduced the room average exposure by 31-66% relative to the baseline case. Some occupant locations were shown to have a higher-than-average exposure, particularly those seated near the airflow outlet, and occupants closest to sources tended to see the highest exposure from said source. We found that these PACs were effective at reducing the stratification caused by overhead heating, and also identified at least one sub-optimal location for placing a PAC in this space.

Keywords: COVID-19, tracer-gas, aerosol, portable-air-cleaner, social distancing, exposure

1. Introduction

The World Health Organization (WHO) [1] and the Centers for Disease Control (CDC) [2] have both concluded that COVID-19 has primarily been spread from person to person

via small respiratory droplets containing virus, particularly in poorly ventilated spaces. The importance of transmission in indoor spaces was highlighted in [3], which surveyed cases across 120 Chinese cities when three or more people were infected and found that all 318 cases they examined occurred indoors. Other detailed studies [4, 5, 6, 7] of different super-spreader events occurring indoors also suggest that airborne transmission was a likely cause of infection; including the case of a Swiss office where 11 of 13 members of a particular team became infected after working in close proximity and reportedly singing 'Happy Birthday' while gathered in a small conference room [8]. All of these examples demonstrate the need to provide building operators with effective strategies to reduce the risk of airborne disease (e.g., COVID-19) transmission in indoor settings.

Computational fluid dynamics (CFD) techniques have been used to investigate the transport and dispersion of respiratory droplets in many environments, with the goal of quantifying and/or reducing transmission risk. These studies include environments such as buses [9, 10], airline cabins [11, 12, 13], classrooms [14, 15, 16], and different hospital settings [17, 18, 19, 20, 21]. Many office scenarios have been studied as well [16, 22, 23], but to the best of our knowledge airborne disease transmission within a small conference room has not been studied. It is critical to understand the transmission patterns in spaces like this where several people gather together in a confined space for an extended period of time. The small conference room noted as a potential spreading location in [8] provides an example of this.

In addition, our literature review found a lack of studies investigating contaminant dispersion or airborne disease transmission in rooms with overhead heating. Liu et al. [24] performed a theoretical analysis on the transport of human speech droplets in thermally stratified rooms. They showed that this stratification can lead to a phenomena referred to as 'lock-up,' where respiratory particles are borne along by buoyant forces at a particular height in the room, contributing to long-range transport of respiratory particles. To our knowledge, no other studies have closely examined the impacts of thermal stratification on contaminant dispersion in a realistic room with overhead heating. For these reasons, we decided to model a conference room with overhead heating, a ventilation strategy particularly known to result in thermal stratification and widely used in many existing buildings.

There are a variety of different mitigation strategies that could be applied to this type of conference room. The American Society of Heating, Refrigerating and Air-Conditioning Engineers (ASHRAE) recommended several mitigation strategies, which have been shown in literature to be effective in limiting airborne disease transmission in indoor spaces. This includes enhanced filtration, upper-room ultra-violet germicidal irradiation (UVGI), local exhaust ventilation, personal ventilation, temperature and humidity control, and the use of portable air cleaners (PACs) [25]. PACs are stand alone units that pull air through high

efficiency particulate air (HEPA) filters, mechanically removing contaminants from the air including virus carrying aerosol particles. We chose to focus on this strategy, for several reasons: PACs 1) are relatively low cost, 2) can be applied in almost any poorly ventilated space, 3) have been shown to be effective at reducing exposure to COVID-19 [26] and have been widely adopted during the pandemic, 4) will likely impact the expected thermal stratification in this space, and 5) have been shown to be effective at improving indoor air quality by reducing other airborne contaminants [27, 28, 29], such as PM_{10}, $PM_{2.5}$, pollen, and more.

Furthermore, previous studies have only modeled a single occupant [17, 18, 19, 22, 23] or a small fraction of the occupants as potential sources [9, 11, 13]. Other studies that model a fuller set of the potential source locations [14, 21] have run separate simulations for each source and only consider one or two air flow conditions. For the purposes of comparing different strategies to generally reduce exposure from an unknown source, it is important to understand how each strategy performs under the full range of possible source locations. It is possible that the level of exposure varies greatly with different source locations, so considering only two or three potential sources could give a misleading representation of a strategy's overall effectiveness in a given space.

To get a more holistic view of the performance of the mitigation strategies within the conference room, we present a modeling strategy to efficiently simulate the contaminant dispersion from multiple potential source locations simultaneously using distinct tracer-gases. Several different flow rates and locations for placing PACs are considered. In addition, we also examine these strategies in both fully occupied and socially distanced room set-ups, since social distancing is another strategy that has been adopted in many buildings. To support our analysis, we also develop a series of metrics to compare the overall performance of different strategies for all the modeled sources and evaluate their location-related performance within the room.

The remainder of this paper is structured as follows. Section 2 describes the CFD model used in this study. Then Section 3 illustrates the case description and Section 4 defines the evaluation metrics. Finally, Section 5 presents the results with the findings summarized in Section 6.

2. CFD Model Description

The CFD simulations were performed using the commercial CFD program ANSYS Fluent 2021 [30]. The following subsections describe the models used for airflow, heat transfer, and contaminant transport.

2.1. Airflow and Heat Transfer Models

The airflow is modeled using a steady-state RNG k-ϵ model. Zhang et al. [31] demonstrated the capability of this type of model to effectively predict airflows and contaminant dispersion in enclosed spaces with forced ventilation, and it has since been used in many similar studies. An ideal-gas equation of state was used to determine the temperature-dependant density of the air-contaminant mixture and link the energy equation to the Reynolds-averaged Navier-Stokes airflow model. Each heat source was assigned a uniform surface heat flux; the radiation flux was calculated using Fluent's P1 radiation model [30] coupled with the energy equation which calculated the convective heat transfer at each surface.

We chose to use a steady-state airflow model in this study for the following reasons. Firstly, we assume that occupants will remain stationary and that the primary flow drivers (i.e., HVAC, PACs, thermal plumes, and the cold-wall) will be constant over the period we are modeling. Also, since our analysis is based on relative differences in steady-state concentration among strategies, any transient effects would be strategy independent, and their potential impact on our relative exposure results would likely be minimal. Finally, steady-state models are significantly less computationally demanding than transient airflow simulations, which allows for the analysis of more release scenarios. We acknowledge however that the use of steady-state models could lead to inaccurate predictions in net exposure particularly over short time periods. In this study we assume that any initial transient period, where the concentration builds to its steady state, is small relative to the total exposure period.

2.2. Contaminant Model

This study used tracer-gases to simulate exhaled virus laden droplet nuclei. Ai et al. [32] outlined three major benefits of these models: 1) airborne disease transmission is primarily caused by the fine droplet nuclei, 2) these fine particles (<3-5μm) can be well represented by tracer-gases in simulations, and 3) tracer-gas simulations are less computationally intensive than other methods, such as Lagrangian particle simulations. For these reasons, many studies have used tracer gases both numerically [9, 13, 18, 22, 23] and experimentally [13, 33] as a surrogate for exhaled viral contaminants. However, these models do not capture the impact of larger particles. Many of which would fall quickly to the ground but some, particularly in the range of 5-20 μm, could carry virus significant distances but behave differently than tracer-gases. This paper does not model the impacts of these differences, assuming their relative effects to be small based on the arguments made in [32] to support reason 1) listed above.

We used an Eulerian species model to simulate the dispersion of an exhaled viral contaminant, which in this case was modeled as the tracer-gas CO_2. The dispersion of the

contaminant was calculated using the following equations:

$$\frac{\partial}{\partial t}(\rho c_i) + \nabla \cdot (\rho c_i \vec{v}) + \nabla \cdot \vec{J}_i = G_i, \tag{1}$$

$$\vec{J}_i = \rho(D_{m,i} + D_t)\nabla c_i - D_{T,i}\frac{\nabla T}{T}, \tag{2}$$

where c_i is the mass-fraction of a particular contaminant i, [%], ρ is the density of the fluid mixture, $\vec{v}$ represents the velocity vector, G_i represents the generation rate of contaminant i, and the term $\vec{J}_i$ represents the diffusive flux of contaminant i. Here $D_{m,i}$ and $D_{T,i}$ are the mass- and thermal-diffusivity coefficients of contaminant i, D_t is the local turbulent-diffusivity coefficient, and T is the local temperature.

This type of model is able to simulate mixtures consisting of many distinct dilute contaminants. In this study we leverage this capability to simultaneously model several different exhaled-virus contaminant sources. Each source emits a distinct tracer-gas which can be used to assess the impact of different source locations on the resulting room contaminant distributions.

2.3. Model Validation

To validate this CFD model's ability to accurately resolve the temperature, velocity, and a tracer gas concentration fields in indoor spaces we simulated an experiment presented in Yin et al. [33], where a tracer gas was released in a single patient hospital ward. We found that our simulated results matched well with the measured data. More details on this model validation and the accompanying mesh independence study can be found in the Appendix.

3. Case Description

3.1. Description of Conference Room

This study examines a model of a hypothetical small conference room. The room dimensions were based on a real conference room measuring 9.1 × 6.1 × 2.7m (30 × 20 × 9ft). The room has a south-facing exterior wall ($x = 9.1$ m), two minor protrusions on the north wall ($x = 0$ m), four asymmetrically-positioned ceiling inlet diffusers, and a single ceiling plenum-return outlet. The single exterior wall was held at a constant temperature of 10°C in all the cases to simulate the heat-loss to the surrounding environment, while the floor, ceiling, and other interior walls were assumed to be adiabatic. The ceiling inlets were modeled as eight-way-throw diffusers with an inlet angle of 35° relative to the ceiling plane, and were based on the momentum definition method described in [34]. In all cases the air is supplied at a constant temperature, 28°C, and a constant flow rate, 0.18 m^2/s (378 cfm). These resulted in the average room air temperatures and velocities ranging from 19.8-21.8

°C and 0.04-0.17 m/s, respectively, with each case falling in the comfortable zone defined by ASHRAE Standard 55 [35].

The fully-occupied room set-up is shown in Figure 1 and consists of 16 occupants seated around a rectangular conference room table with an open center. Each simulated occupant had a laptop, shown in Figure 1. Each occupant and laptop generated 77 and 23 W, respectively, for a total heat load of 100 W per-occupant. Although the virtual thermal manikins we used to simulate the occupants were relatively simple they should provide a good approximation of the thermal plumes on the overall room airflow, other works concerned with the bulk airflow in a given space have used similarly simplified thermal manikins [9, 10, 11, 14, 16, 21, 22, 23, 31, 33]. In a real situation the precise flow induced in a person's micro environment could be greatly influenced by their clothing, body type, posture, and other factors which this work does not consider. To get a sense for the the local contaminant concentrations we measured the average concentrations of each contaminant in each occupant's breath-zone. An individual's breath-zone is defined for this study as the $0.3 \times 0.6 \times 0.6$ m rectangular prism, shown in Figure 1(b), which inscribes a 0.3 m hemisphere centered at a point 76.2 mm (3 in) behind the centroid of the mouth inlet.

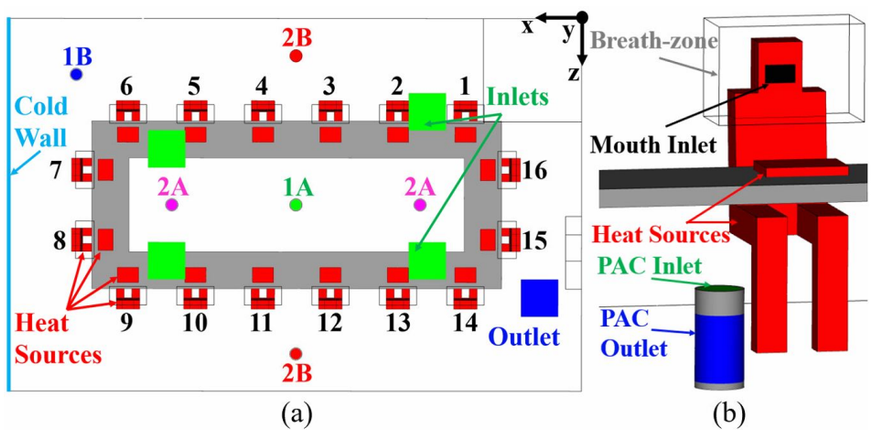

Figure 1: Diagram of the domain boundary conditions including; (a) an overhead view of the fully-occupied room showing the positions of the ceiling inlets and outlet, the different PAC configurations, the cold external wall, and the occupants (numbered 1-16), while (b) shows a close up of one simulated occupants including their breath-zone, and the cylindrical PAC model used in this study. Note that 'dirty' air enters the PAC through the outlet surface (blue) and 100% clean air, $c_i = 0$, enters the room through the inlet surface (green).

3.2. Contaminant Source Model

The tracer-gas source terms used to simulate the exhaled viral contaminants in this study were based on the source term used in [33] and the validation case shown in the Appendix. Tracer-gas solutions of distinct CO_2 contaminants with 1% mass fractions were emitted from the mouth of each source occupant, labeled as Mouth Inlet in Figure 1(b), from each source-i with a contaminant mass-flow of $G_i = 1.9 \times 10^{-6}$ kg/s. To simulate the buoyant effects of

exhaled breath, the mixture leaving each occupant's mouth was modeled at 35°C. For the sake of generality, this study did not attempt to capture the potentially complex momentum source terms that could be generated by an occupant's tidal breathing, talking, or transient events like turning one's head, or coughing. However, we note that these would likely have a limited impact on the over-all steady-state concentration field, as they would mostly be brief phenomena, impart a relatively small amount of momentum to the flow, and primarily have only localized effects near the micro-environment of the source. For this reason, the sources in this study are all released at a negligible velocity of 0.017 m/s normal to the mouth plane.

In reality, the initial momentum of and particle concentration of the virus-laden aerosols source would depend on the respiratory activity the source is engaged in (i.e. talking loudly/softly, breathing, singing) [36, 37]. These differences in momentum would be unsteady, difficult to predict, and would primarily affect the exposure predictions in the region near the source. However, we note that our negligible velocity source would be a fair approximation of an asymptomatic infected person talking or breathing while wearing a mask. Aydin et al. [38] demonstrated experimentally how different mask materials act to retard the velocity of exhaled droplets. And several studies have modeled different masks using CFD techniques [39, 40], demonstrating how masks limit the initial momentum and dispersion of the contaminant. Since masks mandates are now common place in many public indoor spaces, we believe that this negligible velocity source term was appropriate for this analysis of the bulk room airflow and general PAC performance.

3.3. Portable Air Cleaner Model

A simple model of a hypothetical cylindrical PAC was used in this study. The "dirty" air-contaminant mixture, $c_i > 0$, is drawn to the lower portion of the PAC and exits the room through the PAC outlet, labeled in Figure 1(b), which has a uniform surface mass-flux. At the PAC inlet, also labeled in Figure 1(b), 100% clean air, $c_i = 0$, is released into the room with a uniform velocity normal to the surface at the same mass-flow rate and mass-averaged temperature as the flow at the PAC outlet. This model is not intended to represent and particular PAC on the market but rather to represent a fairly common type of nearly-symmetric PAC which draws air from the bottom of the room and inject clean air more or less straight upward.

3.4. Summary of Cases

Summarized in Table 1, this study simulated 18 different cases. We evaluated two room-setups: full-occupied cases with 16 occupants and socially distanced cases with 8 occupants. In both setups, the same eight occupants are modeled as potential sources: the odd-numbered occupants shown in Figure 1(a). We evaluated four different PAC configurations: a single

PAC in two different locations, and two PACs in two different sets of locations. The Association of Home Appliance Manufacturers suggest that the volume flow rate of cleaned air in cubic feet per-minute (cfm) should be equal to 2/3 the area of the room being cleaned in terms of square feet [41]. This gives a recommended clean-air delivery rate (CADR) of 0.189 m^3/s (400 cfm) for the studied conference room, which was found to be a reasonable CADR based on a brief survey of commercially available PACs. For each of the configurations we tested two per-PAC flow rates: a high-flow setting 0.189 m^3/s and a low-flow setting of 0.094 m^3/s (200 cfm), resulting in each configuration being tested at the recommended CADR. These settings are meant to correspond to either a small and medium sized PAC of a similar arbitrary design, or the use of a high and low speed setting. This combination of PAC settings together with the baseline cases gives four different nominal air exchange rates (AERs), with 4.2 air changes per hour (ACH) in the baseline case and 6.4, 8.6, and 13.1 ACH in the PAC cases, which correspond to personal ventilation rates of 11, 17, 23, and 35 L/s/person in the fully occupied cases and twice these values in the socially distanced cases.

Summary of Cases

Room Setup, Occupancy	Portable Air Cleaner Setting	
	Configuration	Flow Rate
Fully Occupied [F], (16 occupants)	No PACs [0]	Low Flow [L], (0.094 m^3/s/PAC)
	1A [1A]	
	1B [1B]	
Socially Distanced [D], (8 occupants)	2A [2A]	High Flow [H], (0.189 m^3/s/PAC)
	2B [2B]	

Table 1: Summary of the cases examined in this work as well as the corresponding abbreviations of each case variable, noted in brackets, used to define and discuss the cases herein.

Table 1 also denotes the short hand used in this study to refer to the different cases within the brackets next to each entry. As an example, the fully occupied case [F] with PAC 1A active [1A] at the high-flow rate [H] will be referred to as F1AH.

4. Evaluation Metrics

4.1. Breath-Zone Concentrations

Each occupant in the conference room is labeled from 1 to m, with m being the total number of occupants in the room. This location numbering for each occupant, previously shown in Figure 1 for the fully occupied case, will be represented by the subscript j. The subscript i will represent the subset of occupants in j being modeled as sources. We can describe i and j in set notation as:

$$j \in [1, 2, ..., m], \quad i \in [s_1, s_2, ...s_n], \quad [s_1, s_2, ...s_n] \subseteq [1, 2, ..., m] \tag{3}$$

where the elements $[s_1, s_2, ...s_n]$ represent the n occupants being modeled as sources and correspond to elements in j.

As noted in Section 3.2, the mass-fraction of each source-i was monitored in each occupant-j's breath-zone, $c_{i,j}$ [%]. We multiplied these mass-fractions by the average density of the ideal-gas mixture in that breath-zone, ρ_j [kg/m^3], and formed a matrix of breath-zone concentrations, $C_{i,j}$ [kg/m^3]. In this paper we will first ignore all the elements of $C_{i,j}$ where $i = j$, because we are not concerned with cases of "self-exposure," where the sick person inhales their own exhaled pathogens. From this breath-zone concentration matrix several averaged values of the breath-zone concentrations can be defined that will be useful in our discussion of these results:

$$CS_i \equiv \frac{1}{m-1} \sum_{j=1, i \neq j}^{m} C_{i,j}, \tag{4}$$

$$CR \equiv \frac{1}{n} \sum_{i=s_1}^{s_n} CS_i = \frac{1}{n(m-1)} \sum_{i=s_1}^{s_n} \sum_{j=1, i \neq j}^{m} C_{i,j}. \tag{5}$$

The values of CS_i represent the room-average breath-zone concentrations of contaminants from a particular source i, excluding the self-exposure scenarios. For brevity, the exposure measures derived from CS_i will be referred to generally as the "source-exposures" or specifically as "source-i's exposure." CR represents the room-average concentration from all the simulated sources in all the measured breath-zones for a given case. Exposure measures using CR will be referred to simply as the "room-exposure" for a particular case, and we will call values normalized by CR "case-normalized exposures"

Similar measures of contaminant concentration from a particular source-i, C_i, and the average concentration of all eight sources, $\overline{C}$, are defined at each point in the domain (rather than specific breath zones). These values will be used in discussing the overall room trends and in the contours and streamlines showing source dispersion paths.

4.2. Why Relative Exposure?

The airborne contaminant concentration an individual is expected to inhale (breath-zone concentration in this study), multiplied by their inhalation rate, and the time that they are inhaling this concentration gives the individual's expected level of exposure to that contaminant. In this paper we focus on reducing exposure generally for an arbitrary time period, rather than, for example, limiting the infections from a given disease over a specified time frame. Such predictions of the expected number of infections in a given scenario are highly dependent upon the amount of virus being exhaled, typically defined in terms of the Wells-Riley quanta generation rate, q, where one *quanta* is equivalent to the expected infectious does of a particular virus [42]. However, q can vary greatly with different pathogens [43] or even between variants of a single virus, as has been seen with the new Delta variant of

SARS-CoV-2 [44]. While there is also variability in q between different individuals, different stages of infection, and during different respiratory activities [36, 37, 45, 46]. In the interest of generality therefore, this paper considers an arbitrary exhaled pathogen and presents the results in terms of the relative level of exposure to that pathogen. We leverage the fact that a dimensionless or normalized measure of the breath-zone concentration is equal to the equivalently normalized value of exposure, for a fixed exposure period and inhalation rate. All of our results will be presented in terms of these dimensionless values of relative exposure.

4.3. Exposure Metrics

For the purposes of normalization, we first define a baseline concentration, C_0. In this study this is the room-averaged concentration, CR, for the baseline case F0. When a breath-zone concentration is normalized by this value it can be thought of as the exposure relative to room average exposure in our baseline case, and will be referred to simply as the "relative exposure." Similarly for other cases, to discuss localized impacts of sources within a given case we will use "case-normalized source exposures," CS_i/CR or C_i/CR.

At other times, the concentration of a given contaminant-i in a breath-zone-j will be normalized by the room average breath-zone concentration from that source. This creates a source-normalized exposure matrix, $C_{i,j}/CS_i$. A key reason for this type of source based normalization is again generality, since each potential source location is equally probable, and the strength of any particular source can vary greatly. It is therefore appropriate to weight the room exposure from each source equally when comparing trends within the room. Thus, to discuss the relative exposure at a particular seat, we define the source-normalized seat-average exposure as follows:

$$(\overline{C_{i,j\neq i}/CS_i})_j = \begin{cases} \frac{1}{n-1} \sum\limits_{i=s_1, i\neq j}^{s_n} \frac{C_{i,j}}{CS_i}, & j \in i; \\ \frac{1}{n} \sum\limits_{i=s_1}^{s_n} \frac{C_{i,j}}{CS_i}, & j \ni i. \end{cases} \tag{6}$$

4.4. Additional Measures

To aid in our discussion of the local impacts of different occupant, source, and PAC locations, we define several distance measures in the xz-plane. First, we define a pair of (x, z) coordinates at the centroid of each occupants contaminant/breath-inlet surface, each PAC inlet surface, and the room outlet surface. Then, for example, the distance from any source-i to any receiving occupant-j, $r_{i,j}$, can be defined as:

$$r_{j,i} \equiv \sqrt{(x_i - x_j)^2 + (z_i - z_j)^2}. \tag{7}$$

Similarly, we can define the horizontal-distance from any source/occupant to the room outlet, $r_{i/j,out}$, or to a given PAC, $r_{i/j,PAC}$. Figure 2 shows an example of each of these measures

with respect to Occupant 3. We will also use the fraction of the contaminant-i being removed by a given PAC, $f_{i,PAC}$ [%], in our discussion of the local impacts of these PACs. This is defined as:

$$f_{i,PAC} \equiv \frac{\dot{m}_{i,PAC}}{G_i}, \tag{8}$$

where $\dot{m}_{i,PAC}$ is the mass-flow rate of contaminant-i out of a given PAC outlet, and G_i is the mass-flow rate at of that contaminant at its source.

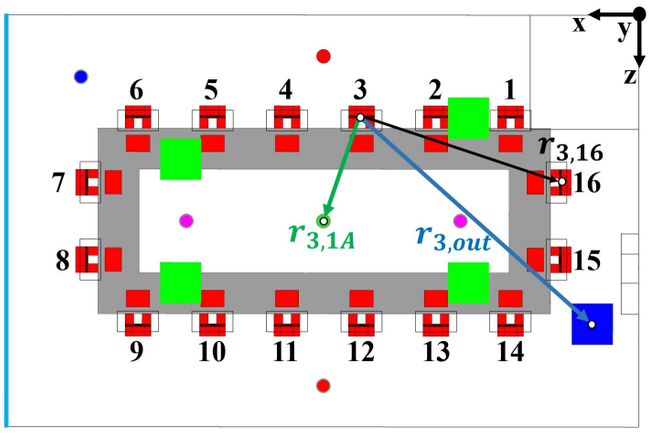

Figure 2: Examples of the radius measures used to discuss the location based trends including the distance from Source 3 to the receiving Occupant 16, $r_{3,16}$ (black), the distance from Source 3 to the room outlet, $r_{3,out}$ (blue), and the distance from the Source 3 to the PAC 1A, $r_{3,1A}$ (green).

To aid in our discussion of thermal stratification in the space, we defined a dimensionless temperature, θ. This is normalized by the volume-averaged temperature of the entire domain for a particular case, T_{avg}:

$$\theta = \frac{T}{T_{avg}}. \tag{9}$$

Finally, it will be useful to discuss how our measures of breath-zone exposure compare to the steady-state concentration in a theoretically well-mixed room, C_{wm} [kg/m^3]. For a room with a total volume flow rate Q_{total} [m^3/s] and a trace gas source of strength G [kg/s], C_{wm} is calculated as follows:

$$C_{wm} = \frac{G}{Q_{total}} = \frac{G}{(Q_{HVAC} + Q_{PACs})}. \tag{10}$$

Each of the four flow rates listed in Section 3.4 has a corresponding well-mixed concentration, and the relative well-mixed exposures, C_{wm}/C_0, will be used in our discussion of stratification.

5. Results and Discussion

In this section, we first discuss the baseline case (without any mitigation strategies) in detail including the major flow features, patterns of contaminant dispersion, and their impacts on the predicted levels of breath-zone exposure. We will then investigate the performance of mitigation strategies under different PAC flow rates, PAC positions, and room setups, across the other cases. Finally, we discuss some of the advantages and limitations of the multiple tracer-gas model used in this study.

5.1. Baseline Case Results

5.1.1. Major Flow Features

Buoyant Mixing

One important flow driver in this space is the human thermal plume [47]. Figure 3 shows the contours of temperature in cross-sections (a) intersecting Occupants 1-6 near their mouth plane and (b) bisecting Occupants 3 and 12. The thermal gradients of the plume coming from the occupants as well as their computers can be seen in Figure 3(b). The resulting strong upward buoyant flows near these heat sources can be seen in the plots of the velocity vectors shown in Figure 4. These distributed sources of momentum in the positive y-direction create a general upward flow throughout the room starting just above the table, with the majority of the downward airflow occurring along the walls of the room, in particular the cold-wall, shown on the left side of Figure 4 (a) and in Figure 5.

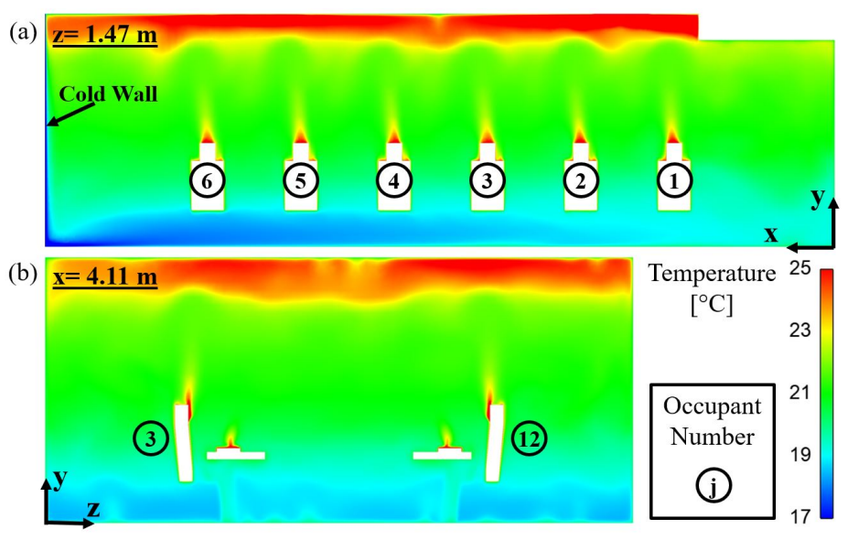

Figure 3: Contours of temperature in the baseline case, F0, showing (a) a plane intersecting Occupants 1-6, 0.01 m from the occupants mouth plane, and (b) the plane bisecting Occupants 3-12.

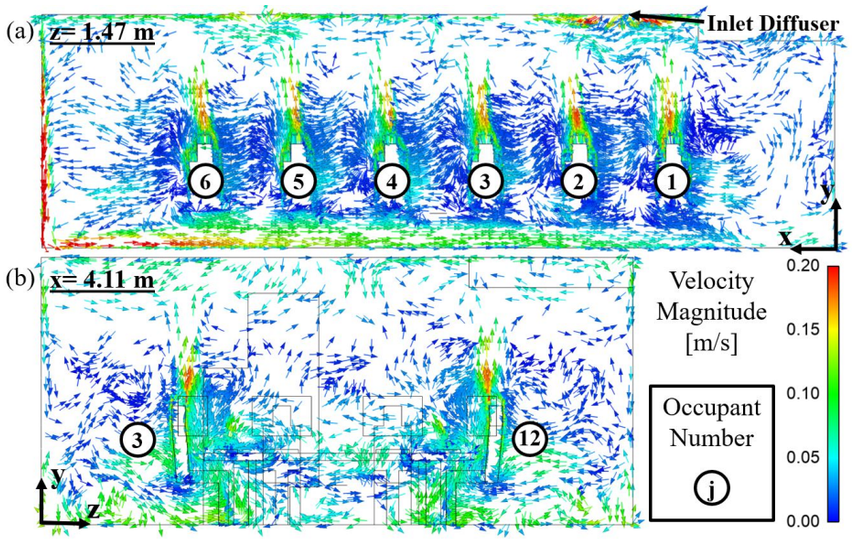

Figure 4: Velocity field in the baseline case, F0, showing (a) a plane intersecting Occupants 1-6, 0.01 m from the occupants mouth plane, and (b) the plane bisecting Occupants 3-12.

Ceiling Boundary Layer

The next important flow feature is the the strong ceiling boundary layer caused by the overhead heating in this room. This region is characterized by a high temperature and high velocity flow almost completely parallel to the plane of the ceiling. It is formed by the strong jets of heated air coming from the inlet diffuser and is only disrupted at points where opposing jets meet and interact. We can see this kind of interaction most clearly in Figure 5 near the mid x-plane where the streamlines from the different inlet diffusers meet and curl downward. The interactions of these jets together with those from the PAC inlets form different "room zones." These zones are characterized by significantly more mixing occurring within a given zone than between two zones. We will discuss this phenomena in more detail in Sections 5.1.3 and 5.2.2.

Short Circuiting

Another important aspect of the flow in this room highlighted by Figure 5 is the significant potential for "short-circuiting" caused by this particular ventilation strategy. The nominal air exchange rate in the baseline case of 4.2 ACH (11 L/s/person) would be considered fairly high for this type of room if it were well-mixed, with the air in theory being fully replaced in under fifteen minutes. However, we can see that a significant fraction of the streamlines flow straight to the outlet without mixing much at all with the bulk air in the room. Many of the streamlines end at the outlet as nearly clean air, $\overline{C}/C_0 \approx 0$, indicating a significant inefficiency in the removal of contaminants from this space. This type of short circuiting could also have negative impacts on the energy efficiency of the heating in this space. Although it is not considered in this work, it would be reasonable to assume that increasing the flow rate of the HVAC system would cause additional short circuiting in the ceiling boundary and corresponding inefficiencies. PACs provide a way to increase the ventilation rates in

rooms like this without adding to the short circuiting, and may also improve the heating performance by increasing mixing in similarly stratified spaces.

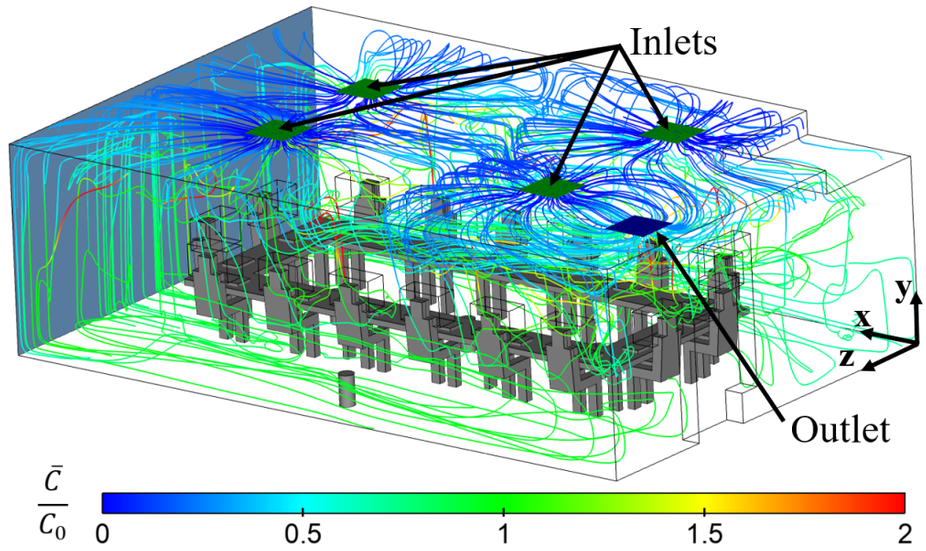

Figure 5: Streamlines starting from the four ceiling inlet diffusers and colored by the average relative concentration, $\overline{C}/C_0$.

Cold Wall

The last major flow driver in this space is the strong buoyancy-driven downward flow along the cold wall. The air in this cold-wall boundary layer accelerates due to gravity as it becomes colder and more dense than the surrounding air. As this downward flow hits the floor, it creates a strong floor boundary-layer which flows in the negative x-direction, and is significantly colder than the air above. The low-temperatures of both the cold-wall and floor boundary layers can be seen clearly in Figure 3, the high velocity in both these regions can be seen in Figure 4, and the streamlines in these regions are shown in Figure 5.

Baseline Case Flow Summary

These flow drivers result in several notable layers forming in this vertically stratified room with overhead heating. First, there is the strong floor boundary layer flowing in the negative x-direction. Above this layer, there is a second layer flowing predominantly in the positive x-direction back towards the cold-wall; these two layers resemble a convective cell at the bottom of the room where air recirculates in a counter-clockwise pattern in the plane of Figure 4(a). The region of lower velocity where these two layers shear against one another stands out in Figure 4. Above this lower room convective cell is a region with more mixing. This mixing region is where we see the generally upward flow caused by the distributed heat sources, the downward flow along the walls, as well as a good amount of chaotic horizontal mixing. Finally, above this mixing region is the ceiling boundary layer characterized by high temperatures, high velocities, and very little vertical mixing at all. This boundary layer in combination with the ceiling plenum return system result in a significant amount of short circuiting in this space, potentially reducing the ventilation effectiveness.

5.1.2. Patterns of Dispersion

Contaminant Stratification

The impact of the thermal plumes on the dispersion of the exhaled viral contaminant is seen clearly in Figure 6, which shows the contours of the average relative-exposure from all eight sources. In general, the human thermal plumes lift the contaminants up and out of the breath-zones of those occupants modeled as sources, see Occupants 1, 3 and 5 in Figure 6. A region of higher concentration accumulates above each source, but below the ceiling boundary layer. This build up of contaminants resembles the lock-up phenomena of contaminants being transported in thermally stratified rooms predicted by one-dimensional models [24].

When we compare the average breath-zone exposure in this baseline case, $CR|_{F0} = C_0$, to the theoretical well-mixed concentration, C_{wm} defined by Equation 10, we find that they are nearly equivalent, $C_{wm}/C_0 = 1.02$. This however is somewhat misleading; since all the occupants in our simulation are seated, none of their breath-zones fall in the high-concentration lock-up region just above their breath-zones. If however one or more of the occupants were standing they could be exposed to this region of higher concentration resulting in a much higher exposure than a well-mixed model would predict. Slightly different thermal profiles or room heights could also cause this lock-up region to occur lower in the room [24] potentially causing much higher exposures in the occupied zone, but we do not consider these complexities in this study.

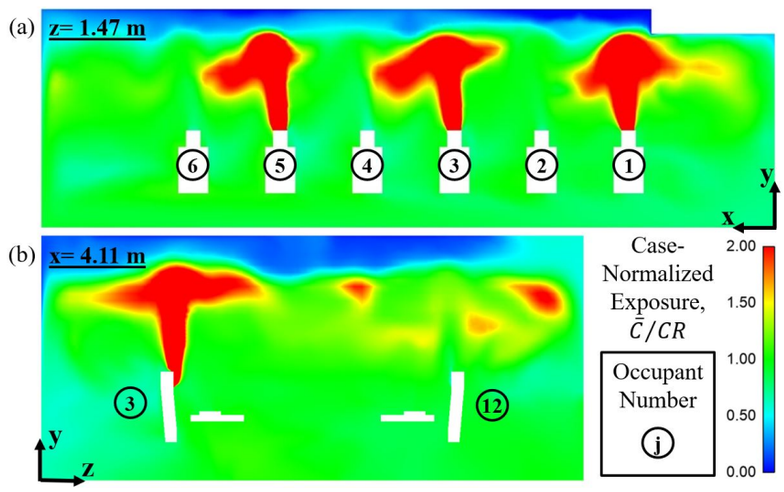

Figure 6: Contours of the room averaged contaminant concentration, $\overline{C}$, normalized by the average breath-zone concentration in the baseline case, F0, showing (a) a plane intersecting Occupants 1-6, 0.01 m from the occupants mouth plane, and (b) the plane bisecting Occupants 3-12.

Source Location

Apart from the common impact of the thermal plumes, the path of dispersion depends greatly on where a contaminant source is located. Figure 7 demonstrates this by comparing the streamlines starting from the mouth inlets of Occupants 1 and 7, both colored by the local

relative-exposure from their respective source. These lines can be thought of as visualizations of the primary path of the momentum-transport of the contaminant and the color can be thought of as a proxy for the diffusive flux of the contaminant away from this primary path. The relative exposure from Occupant 1, $C_1/C_0 = 0.84$, is below the room average, $C_i/C_0 = 1.00$, whereas the exposure for Occupant 7, $C_7/C_0 = 2.64$, is significantly above the average. This is because Occupant 1's close proximity to the outlet leads to a significant portion of the contaminant from that source being transported almost straight to the room outlet. Conversely, Occupant 7's proximity to the cold wall leads to a large portion of the contaminants being transported to the bottom portion of the room, then spread by the strong floor boundary layer across the room. Sun, Li, and Han [47] highlight the potential of human thermal plumes to contribute to the transmission of COVID-19 and other airborne pathogens by helping to lift contaminants from the lower portion of the room up into a persons breath-zone where they can potentially be inhaled. We see this phenomenon clearly in Figure 7(b).

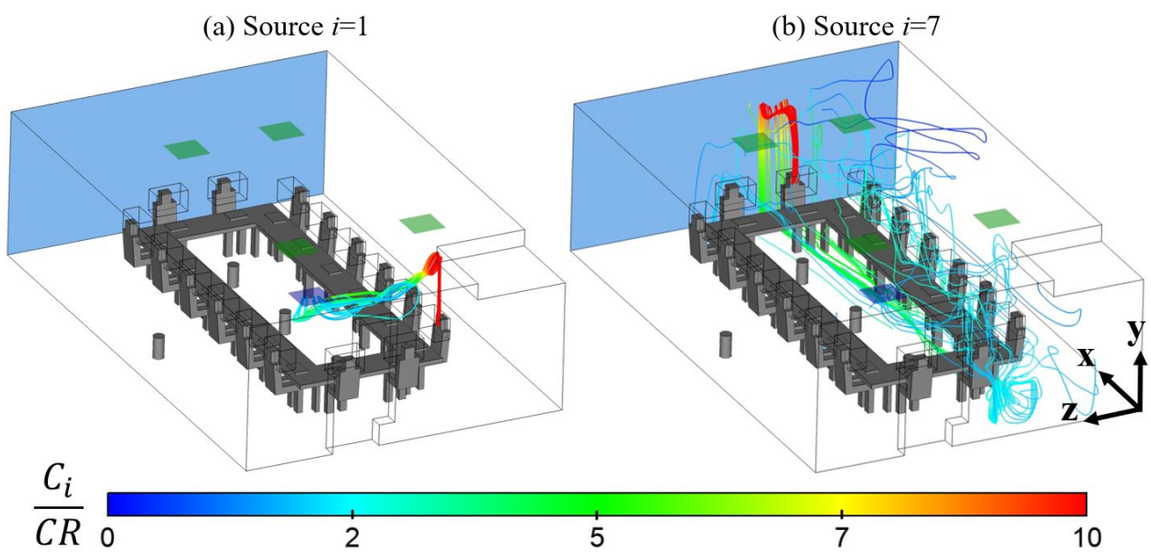

Figure 7: Streamlines of the contaminant dispersion path from source location (a) $i = 1$ and (b) $i = 7$, colored by the local concentration of that source, C_i, normalized by the room average breath-zone concentration from all the sources in this case, CR, referred to as the local case-normalized exposure from that source, C_i/CR.

5.1.3. Breath-Zone Exposure

To discuss several other position related dispersion trends in the baseline case we will use the source-normalized exposure matrix, Table 2. In this table, each row represents the exposures from a particular source-i at each potential receiving breath-zone location j, represented by the columns. Each row is normalized by the room average exposure from that source, CS_i, so that a value of $C_{i,j}/CS_i > 1$ indicates that Occupant-j sees a higher than average exposure from source-i, and similarly $C_{i,j}/CS_i < 1$ indicates below average exposure. The first and most intuitive trend is that the occupants closest to a particular source tend to see the highest exposure from that source. For example, $C_{13,12}/CS_{13} = 2.35$

indicates that Occupant 12 would be expected to see 2.35 times the room-average exposure when Occupant 13, their neighbor, is the source. Similarly, we see this for Occupant 10 when Occupant 11 is the source $C_{12,11}/CS_{12} = 2.17$. However, this general trend is far from absolute; there are several instances when peculiarities in the room airflow pattern can cause the highest breath-zone exposures to occur on the other side of the room from a particular source. For example, when Occupant 7 is the source, a large portion of the contaminant is transported by the cold-wall and floor boundary-layers to the other side of the room, shown in Figure 7(b). This results in Occupant 2 actually seeing the highest exposure from this source, $C_{7,2}/CS_7 = 1.49$, although their neighbor also sees a higher than average level of exposure, $C_{7,6}/CS_7 = 1.43$.

Baseline Case - Source-Normalized Exposure Matrix

$\frac{C_{i,j}}{CS_i}$	Receiving Breath-Zone, j															
Source Location, i	1	2	3	4	5	6	7	8	9	10	11	12	13	14	15	16
1	NA	1.55	1.69	1.52	1.21	1.08	1.12	0.76	0.62	0.59	0.60	0.62	0.67	0.66	0.97	1.33
3	1.19	1.15	NA	1.57	1.62	1.47	1.14	0.81	0.71	0.68	0.68	0.68	0.70	0.66	0.86	1.07
5	1.17	1.23	1.18	1.16	NA	1.39	1.17	0.89	0.84	0.81	0.80	0.79	0.80	0.76	0.91	1.09
7	1.20	1.49	1.32	1.21	1.23	1.43	NA	0.87	0.71	0.67	0.66	0.65	0.66	0.59	0.98	1.32
9	0.36	0.41	0.33	0.30	0.28	0.31	0.64	1.51	NA	1.75	1.77	1.78	1.76	1.74	1.37	0.69
11	0.33	0.37	0.30	0.27	0.26	0.29	0.57	1.29	1.76	2.17	NA	1.84	1.72	2.11	1.17	0.57
13	0.37	0.42	0.34	0.30	0.29	0.32	0.64	1.22	1.50	1.65	2.00	2.35	NA	1.86	1.13	0.62
15	0.51	0.57	0.46	0.42	0.40	0.45	0.89	1.54	1.17	1.15	1.28	1.45	1.80	1.89	NA	1.02
$\overline{(C_{i,j\neq i}/CS_i)}_j$	**0.73**	**0.90**	**0.80**	**0.84**	**0.75**	**0.84**	**0.88**	**1.11**	**1.04**	**1.19**	**1.11**	**1.27**	**1.16**	**1.28**	**1.05**	**0.96**

Table 2: Each row i in the Source-Normalized Exposure Matrix represents the exposures from a particular source-i at each potential receiving breath-zone location j normalized by the room average exposure from that source, CS_i, for the baseline case with fully occupied case with no active PACs (F0). The bottom row shows the source-normalized seat-average exposure, $(\overline{C_{i,j\neq i}/CS_i})_j$, which is the average of the values in the corresponding column j, excluding the instances of self-exposure, $i = j$, marked as 'NA.'

Table 2 also shows how the room tends to be bifurcated into two zones, and occupants tend to see higher than average exposure from the sources in their zone. In the baseline case, this bifurcation occurs along the mid-z-plane with Occupants 1-7 and 16 making up Zone 1, and Occupants 8-15 forming Zone 2. This z-axis bifurcation is largely the result of the interaction of the jets from each pair of inlet diffusers sharing x positions; when these jets meet near the mid-z-plane a significant flow in the negative y-direction is generated and there is not much z-direction mixing across this plane. Meanwhile, the lower-room convective cell provides plenty of x-direction mixing. The interaction of the inlet jets is also less pronounced in the x-direction as the diffusers are spaced farther apart. Finally, to view the overall impact of one's seat location based on all the potential sources, we used the source-normalized seat-average exposure, $(\overline{C_{i,j\neq i}/CS_i})_j$, which takes the average of each column in the source-normalized exposure matrix excluding instances of self exposure. From

this measure we can see that the occupants in Zone 2 consistently see above-average overall exposures as a result of being in the same zone as the room outlet. Since the contaminants from all sources must eventually reach the room outlet, contaminants from Zone 1 must pass through Zone 2, but the reverse is not true.

5.2. Comparison of Results Across Cases

In this section we discuss the general trends observed across the different cases defined in Table 1. We will address each of the major experimental variables examined in this study: PAC flow rate, PAC location, and room set-up (fully occupied and socially distanced).

5.2.1. Impacts of Increasing PAC Flow Rate

All 18 of the cases examined in this study had the same HVAC volume flow rate of 0.178 m^3/s (378 cfm), but there were four different total PAC flow rates tested across these cases: two baseline cases with no PAC flow, four cases at 0.094 m^3/s (200 cfm), eight cases at 0.189 m^3/s (400 cfm), and four cases at 0.378 m^3/s (800 cfm); as described in Table 1. In this section we discuss how several of the trends noted in Section 5.1.2 vary with the different PAC flow rates, including the impacts on stratification, average room-exposure, and the different position based exposure trends.

Thermal and Contaminant Stratification

One major impact of increasing PAC flow rate with this particular PAC design is the reduction of both the thermal and contaminant stratification caused by the overhead heating in this space. To demonstrate this, we show in Figure 8 the plane-averaged values of (a) the normalized temperature, θ, and (b) the average relative exposure, $\overline{C}/C_0$, at different heights, y, averaged over the entire domain for each of the fully-occupied room cases. We can see in Figure 8(a) that increasing the PAC flow rate causes both the region of particularly high temperature at the top of the room and the area of low temperature near the bottom of the room to move closer to the room average temperature, $\theta = 1$. The temperature varies by less than $\pm 5\%$ of the average temperature in the highest flow (0.378 m^3/s) cases compared to about $\pm 16\%$ in the no PAC case.

Figure 8(b) shows that the contaminant stratification is also reduced with increasing PAC flow rate, particularly in the region of highest stratification between the height where the contaminants are released, $y = 1.09$m, and the point of highest exposure, $y = 2$-2.25m. We see in the baseline case (black) that the concentration in this region varies by more than 40% of the reference concentration, C_0, where as in the 0.094, 0.189, and 0.378 m^3/s cases the concentrations vary by 15-32%, 3-12%, and 2-3% of C_0 respectively. We also note that configuration 1B is less effective at reducing this stratification than the other configurations at the same flow rate, and suspect that this is because of PAC 1B's proximity to the fixed

temperature cold-wall. This causes an increase in the convective heat loss to this wall relative to the baseline and other PAC cases, adding to the stratification.

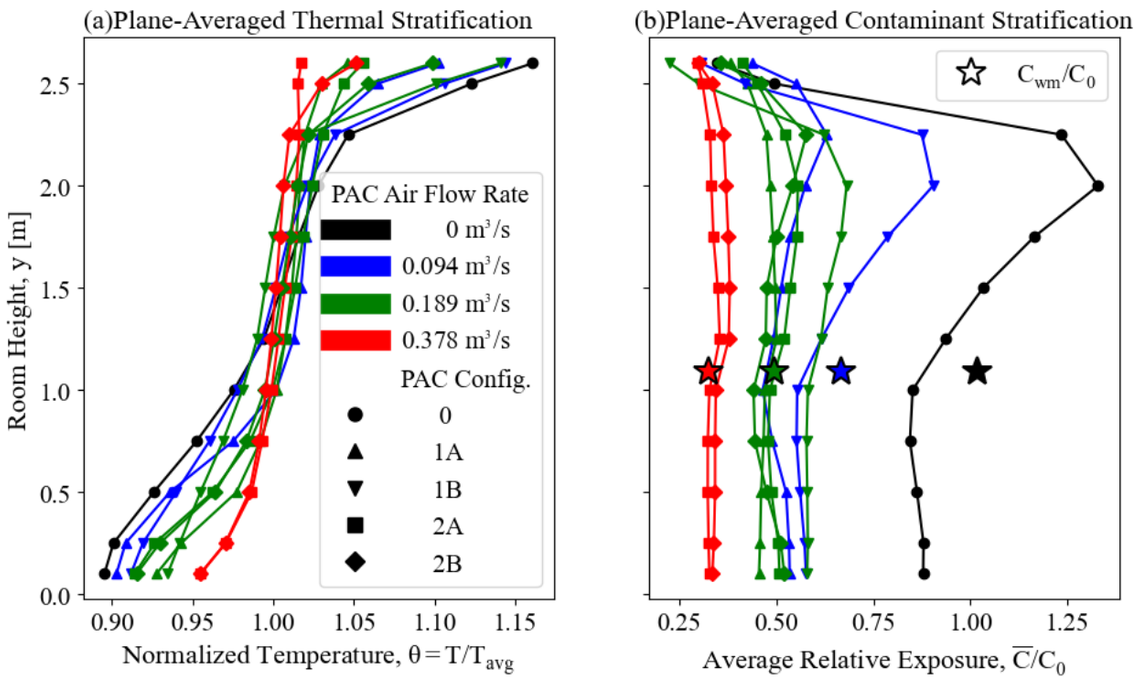

Figure 8: Comparison of the (a) thermal and (b) contaminant stratification across the different PAC settings in the fully-occupied room set-up. The plots show the area-weighted average of their respective quantities for x-z cross-sections of the entire room-domain at the specified height in the room, y. (b) also shows the well-mixed relative exposure, C_{wm}/C_0, for each flow rate, plotted ($\star$) at the midpoint of the measured breath-zone ($y = 1.09$m) for ease of comparison to the exposure measures used in this study.

In Figure 8(b) we also plot the relative well-mixed exposures, C_{wm}/C_0, for comparison to the plane averaged exposures at the level of the breath-zone. We can see in the two most stratified cases F0 (black circles) and F1BL (blue downward-triangles) the plane average exposure at the level of the breath-zones is lower than a well mixed assumption would predict, but is significantly higher in the thermal lock-up region above the breath-zone. As mentioned in Section 5.1.2, this stratification could lead us to underestimate the real exposure in this room if some fraction of the occupants were standing and seeing a higher levels of exposure than the simulated occupants. In the higher flow rate cases, when the room is less stratified and better mixed, this is less true and the well-mixed assumption gives a fairly good approximation of the room exposure in these cases.

Room Exposures

In addition to reducing the the level of stratification in the room, Figure 8(b) also shows how increasing the PAC flow rate also generally reduces the average exposure in the room. We can see that as the PAC flow rate increases the plane-average exposures throughout the room tend to be reduced. Although, for example, case F1AL (blue upward triangles) has lower exposure than F1BH (green downward triangles), it has higher exposure than F1AH (green upward triangles). This is because configuration 1A is more effective than 1B, but

in any configuration increasing the PAC flow rate generally reduces the average exposure throughout the room.

However, these trends become more complex when we consider the breath-zone exposures from individual sources, rather than the general room exposure from all eight sources. We observed several instances where increasing the PAC flow rate changes the room airflow in ways that can increase the breath-zone exposures from particular sources. And occasionally, the sum of these changes results in the average relative breath-zone exposure increasing in the high-flow case relative to the low-flow case. One such instance is shown in Figure 9, which depicts the dispersion paths from two source locations, Occupants 11 and 13, in both (a) the low-flow and (b) the high-flow cases in the socially distanced setup with PAC 1B active. We see in the low-flow case (D1BL) that the dispersion paths from both of these sources lead almost directly to the room outlet, resulting in relative source exposures of $CS_{11}/C_0 = 0.63$ and $CS_{13}/C_0 = 0.15$. In the high flow case (D1BH), on the other hand, the contaminants from these sources are drawn towards the corner with the active PAC, and from there are spread throughout the room. The relative source exposures in this case become $CS_{11}/C_0 = 0.78$ and $CS_{13}/C_0 = 0.79$. Combined, these increases in individual source exposures result in the room average relative concentration increasing from $CR/C_0 = 0.55$ in the low-flow case to $CR/C_0 = 0.62$ in the high-flow case.

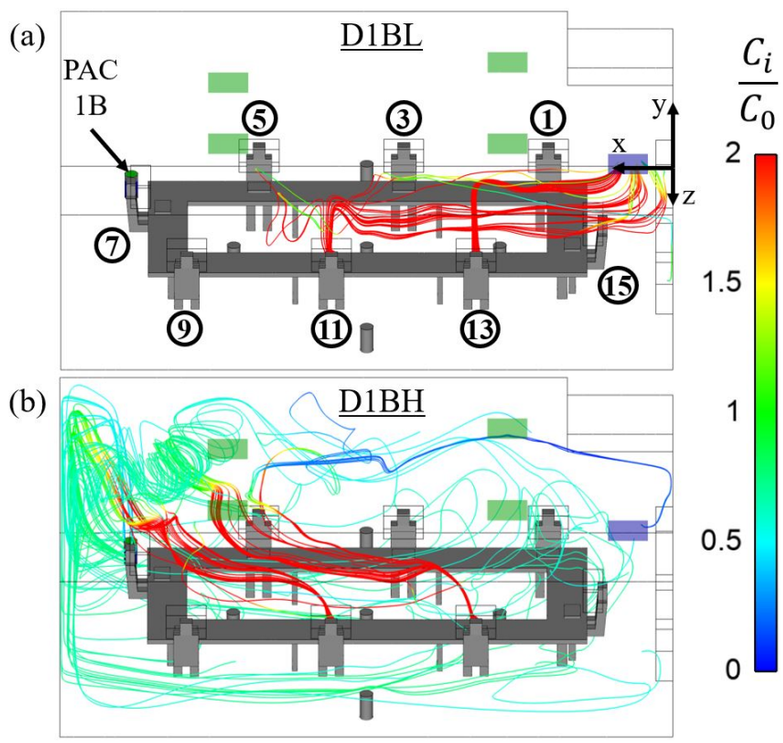

Figure 9: Streamlines of the dispersion path from sources $i = 11$ and 13 for cases (a) D1BL, and (b) D1BH. In each case the streamlines are colored by the respective source-exposures, C_i, normalized by the reference concentration, C_0.

Source Location

In Section 5.1.2 we saw in the baseline case that the relative source exposure depends

greatly upon where in the room the source is located, and that sources closer to the outlet generally cause lower room exposures. We find that both of these trends persisted in the other cases, but were less pronounced with increasing PAC flow rate since the higher flow velocities lead to increased contaminant mixing. Figure 10 demonstrates how the variation due to different source locations is reduced with increasing flow rate, by showing the distribution of the 16 different releases (eight in each set-up) simulated for each PAC setting in a violin plot. The spread of each set is clearly decreasing with increasing flow rate to the point where there is little variation at all when the PAC flow rate is 0.378 m^3/s. Similarly, Figure 11 compares the distance from each source to the room outlet, $r_{i,out}$, to the mean case-normalized exposure from that source for all the cases at a particular PAC flow rate. This shows that this trend too becomes less pronounced with increasing flow rate. There is a clear correlation in the 0 and 0.094 m^3/s cases, and in the 0.189 m^3/s case we see that the source closest to the outlet is still likely to cause below average exposure. However, in the 0.378 m^3/s case there appears to be no correlation. Both of these figures demonstrate the high degree of sensitivity to the source location in the prediction of the room exposure, and clearly show that this sensitivity is reduced as the AER increases and the room becomes more well-mixed.

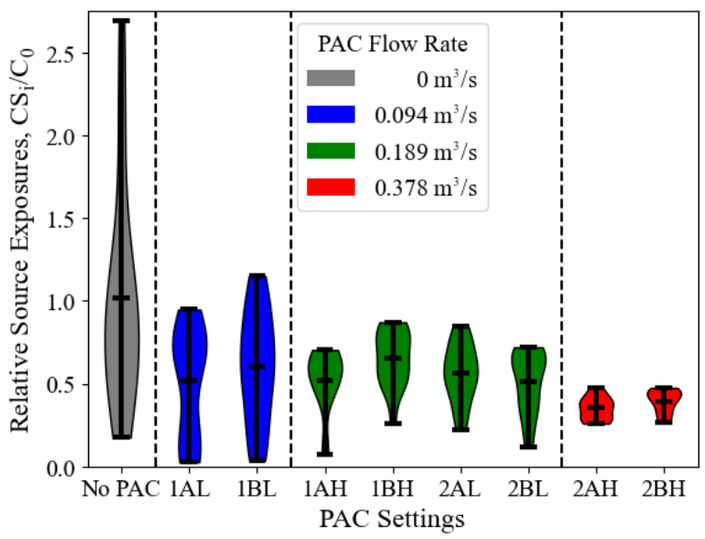

Figure 10: Each violin-plot depicts the distribution of the source exposures, CS_i, relative to the baseline concentration, C_0, at each PAC Setting, with the black lines representing the minimum, mean, and maximum values of each set, and the width representing the distribution of 16 source exposure (8 in each setup) within that range.

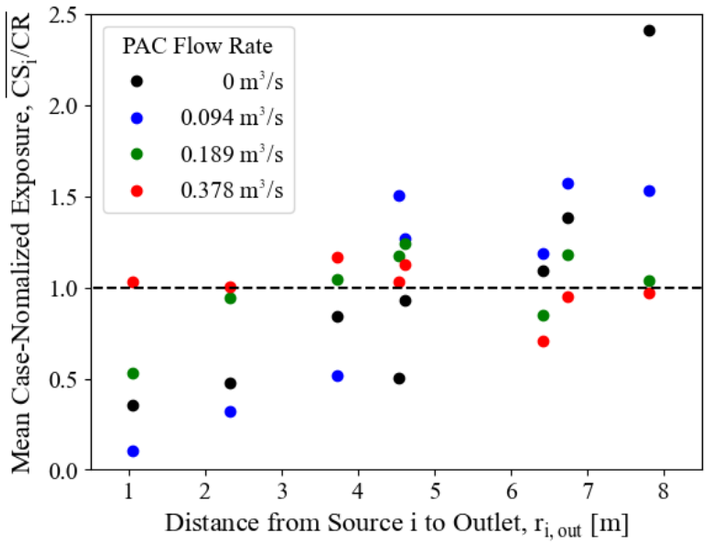

Figure 11: This plot shows the source exposure, CS_i, normalized by the room average exposure for that case, CR. Averaged value at each location i is plotted against the sources distance from the room outlet over all the cases at the same PAC flow rate; 0 m^3/s (black), 0.094 m^3/s (blue), 0.189 m^3/s (green), and 0.378 m^3/s (red).

Proximity to Source

We also noted in Section 5.1.2 that occupants closest to the source tend to see the highest exposure from those sources. This trend is consistent across all flow rates, and is shown clearly in Figure 12. To generate these plots, we matched each individual source-normalized exposure, $C_{i,j}/CS_i$, with the corresponding distance from that source to the receiving breath-zone, $r_{i.j}$. Then, for each PAC flow rate, we took the average of all these exposures at each value of $r_{i,j}$. We can see from this figure that on average occupants within about $r_{i,j} = 2.2$m consistently see higher than average exposures from that source ($(\overline{C_{i,j}/CS_i})_{r_{i,j}} > 1$). It is also important to note that the tracer gas model may under predict this relative exposure near the source. A more complex source which considered the contribution of larger particles ($> 5\mu$m), would likely predict even higher levels of exposure in the near-field region, as well as an increased risk of fomite transmission from large deposited particles nearer to the source.

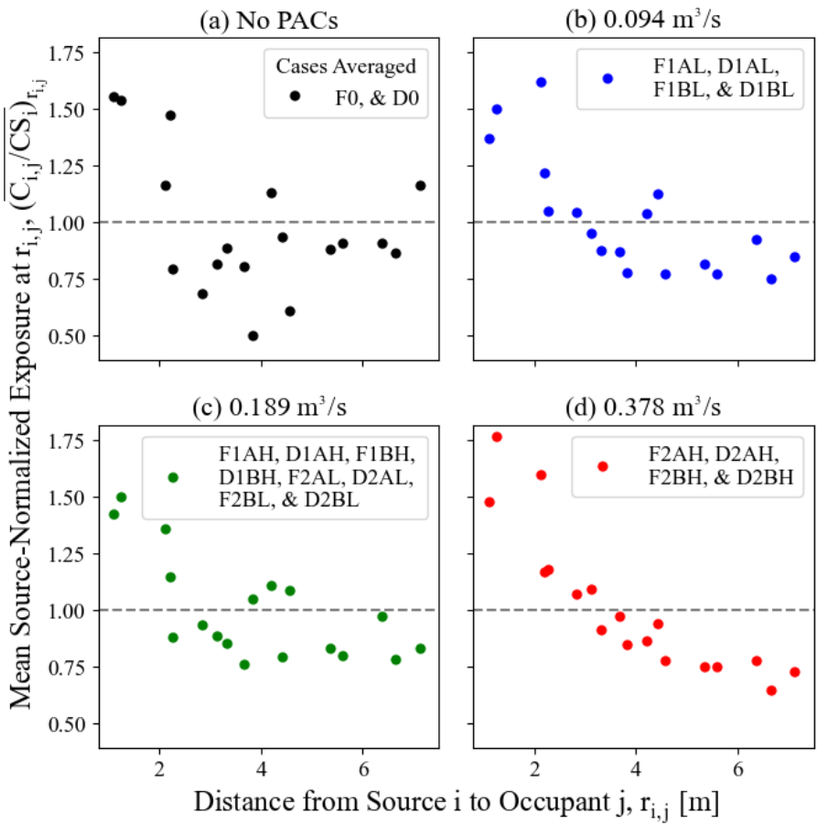

Figure 12: The individual exposures, $C_{i,j}$, which have the same distance from the source to the receiving occupant, $r_{i,j}$, each normalized by the average exposure from the corresponding source, CS_i, averaged over all the cases at a particular PAC flow rate: (a) 0 m^3/s, (b) 0.094 m^3/s, (c) 0.189 m^3/s, and (d) 0.378 m^3/s. $(\overline{C_{i,j}/CS_i})_{r_{i,j}} > 1$ indicates a higher-than-average exposure at the distance $r_{i,j}$ from the source-i across all cases at that flow rate.

5.2.2. Impacts of PAC Location

Optimizing Position

Although finding an optimal location was outside the purpose of this paper, we were able to identify one sub-optimal PAC configuration, 1B. Figure 13 compares the room average relative exposure in all 18 of the cases tested. We see that in both the fully-occupied and socially distanced setups the 1BL cases see higher exposures than the other 0.094 m^3/s flow rate cases, and the 1BH cases both see higher exposure than all the other 0.189 m^3/s cases. Of the other three configurations, none stand out. For example, configuration 2A sees higher exposure than 2B in the low-flow cases, but lower exposure in the high-flow rate cases. We also found no significant benefit to using two PACs rather than a single PAC for the same total CADR. We see in Figure 13 that for the 1AH cases are only slightly better than the 2AL cases and essential equivalent to the 2BL cases.

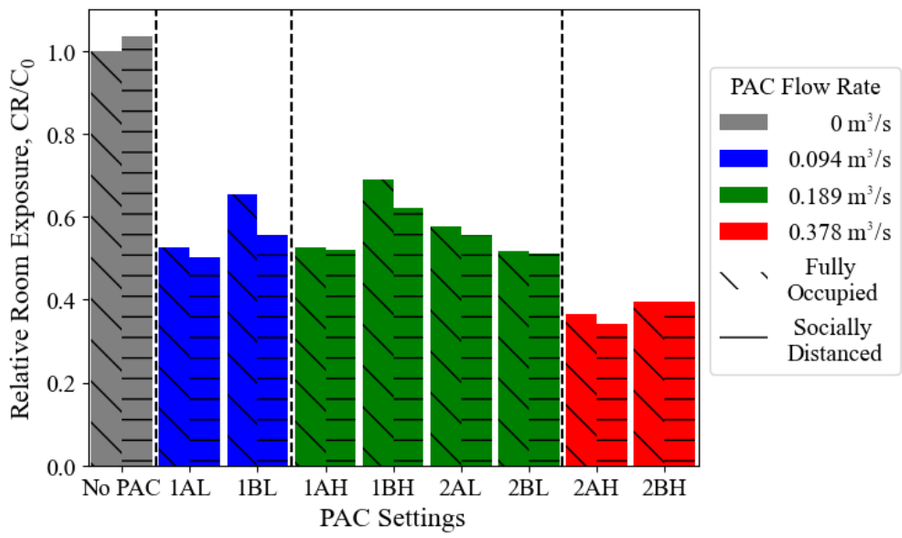

Figure 13: Histogram of the room average breath-zone concentrations in each case, CR, normalized by the baseline concentration, C_0.

Proximity to PAC

We found no significant relationship between proximity to a given PAC and relative exposure. We first considered the impact of sitting closer to a particular PAC, but found no relationship between an occupant's source-normalized seat-exposure, $(\overline{C_{i,j\neq i}/CS_i})_j$, and the distance from that occupant to the active PAC, $r_{j,PAC}$. Similarly, we found no notable trends with respect to a source-i's proximity to the active PAC, $r_{i,PAC}$; neither the case-normalized room exposure from that source, CS_i/CR, nor the removal fraction of contaminant-i by that PAC, $f_{i,PAC}$, showed a consistent relationship to $r_{i,PAC}$. This is largely a result of the particular PAC model we used in this study, and Figure 14 shows why. The jet of contaminant-free air from the PAC inlet is directed straight up, rather than at a 45°angle, for example, which might direct some portion of this clean air into near-by occupants' breath-zones. Consequentially, these PACs do not provide any significant benefit to healthy people nearby, but a different PAC design might. In a few instances, a source sitting near an active PAC actually spreads the contaminant around the room more effectively, increasing the room exposure from that source. Figure 15(b) shows an example of this, Occupant 5 in case F2AL is seated close to an active PAC, but hardly any of the streamlines from this source lead to that PAC outlet and are instead effectively dispersed throughout the right side of the room, resulting in a high case normalized exposure from this source, $CS_5/CR = 1.2$.

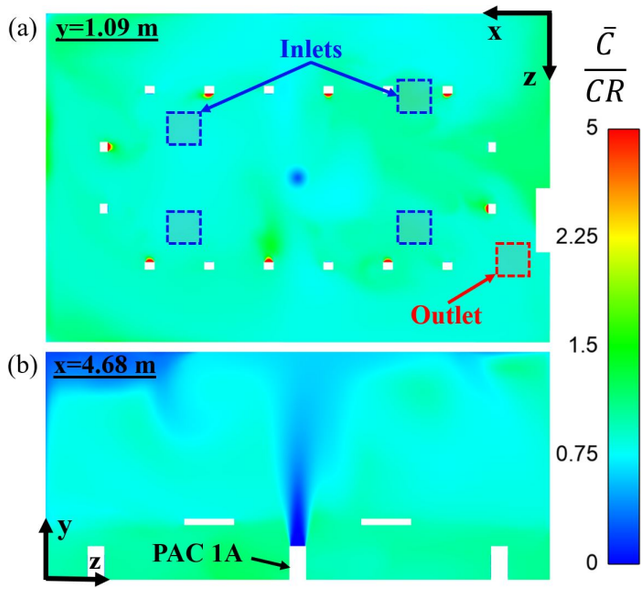

Figure 14: Contours of the average contaminant concentration from all eight sources, $\overline{C}$, normalized by the room average breath-zone exposure, CR, for case F1AL shown at (a) the occupants breath-plane at the center of each mouth inlet, and (b) the mid-plane of the room bisecting PACs 1A and 2B.

Room Zones

We also found that the position of the PACs can impact how the room zones form in this space. Several of the PAC configurations, namely the 2A, 2B, and low-flow 1A case, form the same z-axis bifurcated room zones as in the baseline cases, shown in Table 2 for F0. In the high-flow rate 1A cases however, the room is bifurcated along the mid-x-plane. Figure 15 compares the dispersion path from one source, Occupant 5, in two different cases. Figure 15(a) shows case F1AH when the room is bifurcated along the x-axis mid plane. Here the streamlines show that there is very little dispersion of contaminant along the room's x-axis. Instead, there ends up being a large amount of recirculating contaminant in the immediate vicinity of Occupant 5, and some dispersion around the zone consisting of Occupants 4-11. Figure 15(b) on the other hand shows case F2AL, where the room is bifurcated along the z-axis mid plane. We see in this case that there is much more x-direction mixing and limited mixing in the z-direction. As in the baseline case, in addition to seeing higher than average exposure from occupants in their zone, occupants in the same zone as the outlet tend to see a slightly higher exposure overall. This is due to the contaminants from the other zone leaving their zone to reach the room outlet. Figure 15(b) demonstrates this phenomena, as we can see several streamlines passing into the other zone, towards the room outlet.

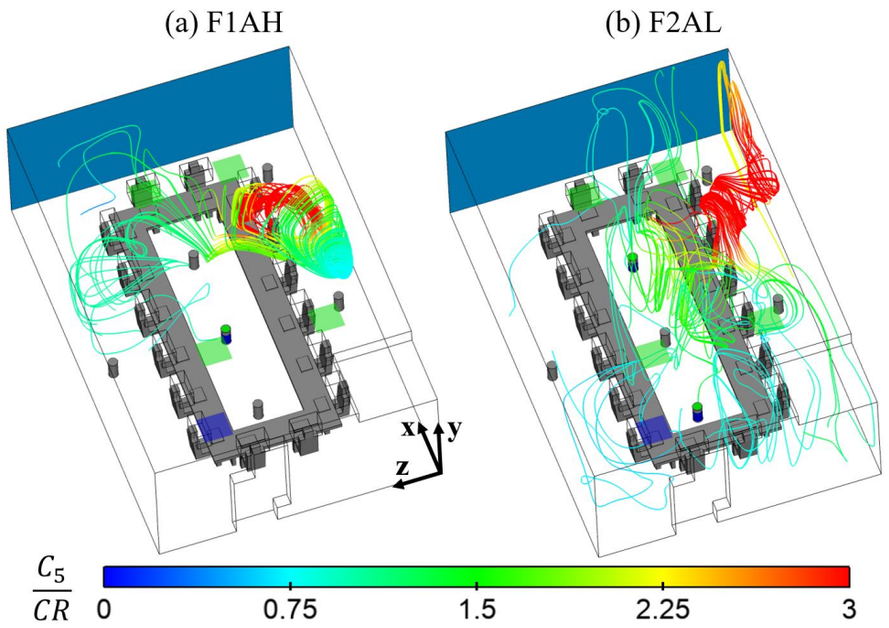

Figure 15: This figure shows streamlines of the dispersion path of the contaminant from Occupant 5 colored by the local concentration of contaminant-5, C_5, normalized by the room average breath-zone exposure, CR, for (a) case F1AH when the room is bifurcated along the x-axis direction, and (b) case F2AL when the room is bifurcated along the z-axis.

5.2.3. Impacts of Room Set-up

Benefits of Social Distancing

It should first be noted that social distancing reduces the likely hood of transmission via the direct inhalation of large ballistic (non-aerosolized) droplets as well as the potential fomite transmission due to these or other droplets being deposited on surfaces in the room. This study considers only the airborne or aerosol transmission route. The most significant benefit of the socially-distanced room setup in reducing airborne transmission comes from reducing the number of susceptible occupants being exposed to a potentially asymptomatic source of airborne virus. Assuming there is one infected person and all others are susceptible, implementing social distancing would reduce the number of susceptible people in the room from 15 to 7, which for the same room average exposure would reduce the expected number of infections correspondingly by 53%.

In addition to this benefit, we find that there also tends to be a slight reduction in the room average exposure in the socially distanced cases. In Figure 13, we can see that, for all the cases with PACs, the relative exposure is slightly lower in the socially distanced case for the same PAC setting. We suspect that this is related to our observation above, that occupants closer to a source tend to see higher than average exposure. As the additional occupants in fully-occupied set-up cause more people to be in the $r_{i,j} < 2.2$ m region of higher than average exposure it makes sense that the relative level of exposure is slightly higher in these cases. With PAC settings 1AL, 1AH, 2AL, 2BL, and 2BH the difference is very slight with $< 5\%$ reduction in the distanced case. The only exception to this trend is

the No PACs setting. Figure 13 shows that the socially distanced no PAC case has a slightly higher, 3.4%, room average exposure than the baseline fully-occupied no PAC case (F0). We suspect that this is because the added upward momentum of the additional thermal plumes, which help to lift the contaminants out of the occupant's breath-zones, strengthening both the thermal and contaminant stratification. By comparison, in the cases with PACs, the higher room average velocities mean that the slight upward velocity induced by the thermal plumes is relatively less influential, and the added vertical mixing from the PACs helps to break up the stratification.

Changes in Airflow

For the several settings with larger differences between the fully occupied and distanced cases, we noticed that the changes to the room set-up caused major differences in the overall room airflow and the resulting dispersion pattern. Figure 16 highlights the difference in the airflow pattern between the fully occupied and socially distanced cases with the 1BL PAC setting. It shows the streamlines of the air coming from the PAC inlet colored by the local flow's velocity magnitude. We see in D1BL that there is a strong flow which passes in between Occupants 3 and 5, then continues on through the center of the room, bringing more fresh air into the the Occupant's breath-zones than in case F1BL, where this flow is disrupted by the presence of Occupant 4.

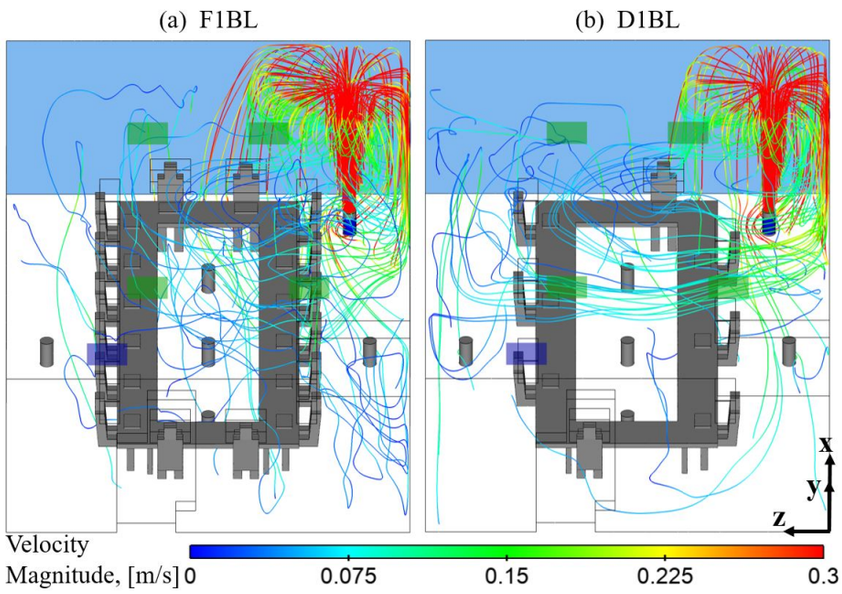

Figure 16: Comparison of the streamlines, colored by the local velocity magnitude, coming from the PAC inlet in (a) the fully occupied and (b) the socially distanced room setups for the PAC setting 1BL.

5.3. Discussion

In this section we will discuss some of the major findings and identify which can be applied more broadly and which are specific to the type of case we studied here. For example, we showed that the room set-up (source location, seating arrangement, PAC setting, HVAC inlets/outlets) can have a significant impacts on the flow paths that develop in a particular

room, and note that in general as flow rates increase and the room becomes more well-mixed the influence of local factors (i.e. source location) have less of an impact on the room-average exposure prediction. Of course, the flow paths for a specific case will depend on the set-up of the room in question, but our observations that occupants see higher levels of exposure when seated closer to the source and in the path from the source to the outlet, should apply to most scenarios.

The specific PAC design and how it interacts with the room airflow are important factors in understanding the overall performance of a PAC in a particular room. We note that the type of PAC studied here, which draws air from the bottom of the room and directs it straight upward, is particularly suited to similar rooms with high levels of thermal stratification. The added vertical mixing provided by these PACs helps to improve the heating efficiency, and also reduces the contaminant build-up in the upper portion of the room caused by thermal lock-up. We also note that in general PACs are a particularly good strategy for rooms where there is significant short circuiting since they can be used to increase the ventilation rate without adding to the inefficiencies of an existing ventilation strategy, and improving the ventilation effectiveness.

Efficient CFD methods are needed to evaluate the in-room performance of different ventilation strategies, PAC designs, and other risk mitigation strategies. The steady-state methods we used are particularly suited to similar cases with constant airflow, occupancy, and source strengths as well as relatively long exposure periods (conference rooms, classrooms, and offices for example). These techniques may be less applicable in situations with more transient boundary conditions, or in large rooms that never reach a steady-state. Similarly, the multiple tracer-gas technique and the breath-zone based relative exposure metrics developed in this study are particularly suited for comparing the relative performance of different mitigation strategies aimed at improving the ventilation in a given space. This technique enables the efficient assessment of a strategies performance under different release scenarios to provide a more holistic view of its overall performance. For studies focused on aspects such as particle deposition, evaporation, and the contribution of larger particles ($> 5\mu$m) to the exposure, Lagrangian contaminant models may be more appropriate. And for studies focused on limiting the number of infections of a particular disease over a specified period, rather than generally reducing the exposure to an arbitrary pathogen, Wells-Riley type infection predictions would be more suitable than the measures of relative exposure used in this study.

6. Conclusion

This study used a multiple-tracer-gas CFD technique to holistically assess the impact of several PAC configurations on relative exposure to an arbitrary aerosol source. To our knowl-

edge, this was the first such investigation of contaminant dispersion in a small conference-room, or in a room with over-head heating. We evaluated four different PAC configurations, four different total PAC flow rates, and both fully-occupied and socially distanced room setups. The following conclusions are drawn about this space:

- Overhead heating leads to thermal stratification in this space and a build-up of exhaled contaminants in the region just above the measured breath-zones.
- The increased vertical mixing caused by the PACs studied here helps to reduce both the thermal stratification and the resulting contaminant stratification in this space.
- Where a person sits can impact their average exposure. Occupants seated in same zone as a particular source, in the path of that source to the outlet, and particularly those within 2.2 m of the source all tend to see a higher than average exposure from that source.
- The location of a source within a room can dramatically impact the room-average exposure from that source. Sources closer to the room outlet tend to cause a lower level of exposure, while sitting next to a strong flow driver such as the cold-wall or in some cases the flow from the active PAC can help to spread contaminants around the room causing a higher level of exposure.
- The sensitivity of the room-average exposure to the source location is reduced with increasing PAC flow rate. The highest flow-rate cases result in the room being close to well-mixed and therefore reduce the dependence on source location.
- Increasing PAC flow rate in general reduces the room average exposure, but occasionally differences in the room airflow can increase exposure from particular source locations. These differences in dispersion pattern can lead to some cases with higher flow rates having higher average breath-zone exposures.
- Changes to the PAC configuration or room set-up can significantly change the room air-flow pattern and the resulting effectiveness of the PAC at reducing exposure.

Of the four PAC configurations examined here, we found at least one that was sub-optimal, location 1B when the PAC was placed in the corner of the room. Across the cases studied we found on average that the level of room exposure was reduced by 45, 44, and 63% relative to the no PAC cases for the cases with PAC flow rates 0.094, 0.189, and 0.378 m^3/s cases respectively. We didn't identify any significant difference in using one PAC with high flow rate versus two PACs with low flow rate if the total flow rates are the same. But did find that across the cases increasing the PAC flow rate reduced both the mean exposure in the room

and the variability in the room exposures due to source location. Although we were unable to determine an optimal PAC location, we did identify several aspects that would be critical to finding an optimal PAC position including especially the room set-up and the location of the room outlet; and we demonstrated how the multiple tracer-gas technique could be used to assess and compare the in-room performance of different mitigation strategies.

Acknowledgments

This research was supported in parts by the U.S. Defense Threat Reduction Agency and performed under U.S. Department of Energy Contract No. DE-AC02-05CH11231, and by a summer research fellowship provided by the Department of Mechanical Engineering at the University of Colorado Boulder. We would like to thank Dr. Yonggao Yin for providing us with the experimental data used to validate our model, and would also like to thank ANSYS Inc. who provided us with the software licenses used for this study.

References

1. World Health Organization. QA on coronaviruses (COVID-19), How does COVID-19 spread between people? 2020. https://www.who.int/emergencies/diseases/novel-coronavirus-2019/question-and-answers-hub/q-a-detail/coronavirus-disease-covid-19-how-is-it-transmitted. Accessed 24 Oct 2020.

2. Centers for Disease Control and Prevention. Frequently Asked Questions on Coronavirus 2020. https://www.cdc.gov/coronavirus/2019-ncov/faq.htmlSpread Accessed 24 Oct 2020.

3. Qian H, Miao T, Liu L, Zheng X, Luo D, Li Y. Indoor Transmission of SARS-CoV-2. *Indoor Air.* 2020;31(3):639-645.

4. Miller S, Nazaroff W, Jimenez J, *et al.* Transmission of SARS-CoV-2 by inhalation of respiratory aerosol in the Skagit Valley Chorale superspreading event. *Indoor Air.* 2021;31:314–323.

5. Lu J, Gu J, Li K, *et al.* COVID-19 Outbreak Associated with Air Conditioning in Restaurant, Guangzhou, China, 2020. *Emerging Infectious Diseases.* 2020;26(7):1628-1631.

6. Lendacki F, Teran R, Gretsch S, Fricchione M, Kerins J. COVID-19 Outbreak Among Attendees of an Exercise Facility — Chicago, Illinois, August–September 2020. *Morbidity and Mortality Weekly Report.* 2021;70(9):321–325.

7. Vernez D, Schwarz S, Sauvain J, Petignat C, Suarez G. Probable aerosol transmission of SARS-CoV-2 in a poorly ventilated courtroom. *Indoor Air.* 2021.

8. Weissberg D, Böni , J. , *et al.* Does respiratory co-infection facilitate dispersal of SARS-CoV-2? investigation of a super-spreading event in an open-space office. *Antimicrobial Resistance Infection Control.* 2020;9.

9. Zhu S, Srebric J, Spengler J, Demokritou P. An advanced numerical model for the assessment of airborne transmission of influenza in bus microenvironments. *Building and Environment.* ;47:67-75.

10. Yang X, Ou C, Yang H, *et al.* Transmission of pathogen-laden expiratory droplets in a coach bus. *Journal of Hazardous Materials.* 2020;397(122609).

11. Yan Y, Li X, Shang Y, Tu J. Evaluation of airborne disease infection risks in an airliner cabin using the Lagrangian-based Wells-Riley approach. *Building and Environment.* ;121:79-92.

12. Han Z, To S, Fu S, Chao C, Weng W, Huang Q. Effect of human movement on airborne disease transmission in an airplane cabin: study using numerical modeling and quantitative risk analysis. *BMC Infectious Diseases.* 2014;14(434).

13. Li B, Duan R, Li J, *et al.* Experimental studies of thermal environment and contaminant transport in a commercial aircraft cabin with gaspers on. *Indoor Air.* 2016;26:806–819.

14. Abuhegazy M, Talaat K, Anderoglu O, Poroseva S. Numerical investigation of aerosol transport in a classroom with relevance to COVID-19. *Physics of Fluids.* 2020;32(103311).

15. Ascione F, De Masi R, Mastellone M, Vanoli G. The design of safe classrooms of educational buildings for facing contagions and transmission of diseases: A novel approach combining audits, calibrated energy models, building performance (BPS) and computational fluid dynamic (CFD) simulations. *Energy and Buildings.* 2021;230(110533).

16. Lee K, Zhang T, Jiang Z, Chen Q. Comparison of airflow and contaminant distributions in rooms with traditional displacement ventilation and under-floor air distribution systems. *ASHRAE Transactions.* 2009;115:306-321.

17. Qian H, Li Y, Nielsen P, Huang X. Spatial distribution of infection risk of SARS transmission in a hospital ward. *Building and Environment.* 2009;44:1651–1658.

18. Hang J, Li C, W.H. J, Jin R, Liu L, Xie X. Potential airborne transmission between two isolation cubicles through a shared anteroom. *Building and Environment.* 2015;89:264–278.

19. Hou M, Pantelic J, Aviv D. Spatial analysis of the impact of UVGI technology in occupied rooms using ray-tracing simulation. *Indoor Air.* 2021;126:220-228.

20. Buchan A, Yang L, Atkinson K. Predicting airborne coronavirus inactivation by far-UVC in populated rooms using a high-fidelity coupled radiation-CFD model. *Scientific Reports.* ;10.

21. King MF, Noakes C, Sleigh P. Modeling environmental contamination in hospital single- and four-bed rooms. *Indoor Air.* 2015;25:694–707.

22. Barbosa B, De Carvalho Lobo Brum N. Ventilation mode performance against airborne respiratory infections in small office spaces: limits and rational improvements for Covid-19. *Journal of the Brazilian Society of Mechanical Sciences and Engineering.* 2021;43.

23. Eldegwy A, Sobhi M, Khalil E. CFD application to improve infection control in office rooms. *ASHRAE Transactions.* 2020;126:220-228.

24. Liu F, Qian H, Luo Z, Zheng X. The impact of indoor thermal stratification on the dispersion of human speech droplets. *Indoor Air.* ;31:369–382.

25. American Society of Heating, Refrigeration and Air Condition-ing Engineers. ASHRAE Position Document on Infectious Aerosols 2020.

26. Lindsley WG, Derk RC, Coyle JP, *et al.* Efficacy of Portable Air Cleaners and Masking for Reducing Indoor Exposure to Simulated Exhaled SARS-CoV-2 Aerosols — United States, 2021. *MMWR and Morbidity and Mortality Weekly Report.* 2021;70:972–976.

27. Cheek E, Guercio V, Shrubsole C, Dimitroulopoulou S. Portable air purification: Review of impacts on indoor air quality and health. *Science of The Total Environment.* 2021;766(142585).

28. Curtius J, Granzin M, Schrod J. Testing mobile air purifiers in a school classroom: Reducing the airborne transmission risk for SARS-CoV-2. *Aerosol Science and Technology.* 2021;55:586-599.

29. Cox J, Isiugo , K. P, *et al.* Effectiveness of a portable air cleaner in removing aerosol particles in homes close to highways. *Indoor Air.* 2018;46:818–827.

30. ANSYS Incorporated. Fluent 2020 R1 Theory Guide 2020. https://ansyshelp.ansys.com/account/secured?returnurl=/Vie

31. Zhang Z, Zhang W, Zhai Z, Chen Q. Evaluation of Various Turbulence Models in Predicting Airflow and Turbulence in Enclosed Environments by CFD: Part 2—Comparison with Experimental Data from Literature. *HVACR Research.* 2007;13:871–886.

32. Ai Z, Mak , C.M. , Gao N, Niu J. Tracer gas is a suitable surrogate of exhaled droplet nuclei for studying airborne transmission in the built environment. *Building Simulation.* 2020;13:489–496.

33. Yin Y, Xu W, Gupta J, *et al.* Experimental Study on Displacement and Mixing Ventilation Systems for a Patient Ward. *HVACR Research.* 2009;15:1175–1191.

34. Srebric J, Q. C. Simplified Numerical Models for Complex Air Supply Diffusers. *HVACR Research.* 2002;8:277-294.

35. American Society of Heating, Refrigerating and Air-Conditioning Engineers. ASHRAE Standard Thermal Environmental Conditions for Human Occupancy. Atlanta, Ga. :The Society, 1992.

36. Gregson FKA, Watson NA, Orton CM, *et al.* Comparing aerosol concentrations and particle size distributions generated by singing, speaking and breathing. *Aerosol Science and Technology.* 2021;55(6):681-691.

37. Coleman KK, Tay DJW, Tan KS, *et al.* Viral Load of SARS-CoV-2 in Respiratory Aerosols Emitted by COVID-19 Patients while Breathing, Talking, and Singing. *Clinical infectious diseases : an official publication of the Infectious Diseases Society of America.* 2021.

38. Aydin O, Emon , B. C, *et al.* Performance of fabrics for home-made masks against the spread of COVID-19 through droplets: A quantitative mechanistic study. *Extreme Mechanics Letters.* 2020;40(100924):421-432.

39. Leonard S, Strasser W, Whittle J, *et al.* Reducing aerosol dispersion by high flow therapy in COVID-19: High resolution computational fluid dynamics simulations of particle behavior during high velocity nasal insufflation with a simple surgical mask. *Journal of the American College of Emergency Physicians Open.* 2020;1:578–591.

40. Dbouk T, Drikakis D. On respiratory droplets and face masks. *Physics of Fluids.* 2020;32(063303).

41. Association of Home Appliance Manufacturers. Air Filtration Standards 2021. https://ahamverifide.org/ahams-air-filtration-standards Accessed 26 July 2021.

42. Riley E, Murphy G, Riley R. Airborne spread of measles in a suburban elementary school. *American Journal of Epidemiology.* 1978;107(5):421-432.

43. Zemouri C, Awad , S.F. , *et al.* Modeling of the Transmission of Coronaviruses, Measles Virus, Influenza Virus, Mycobacterium tuberculosis, and Legionella pneumophila in Dental Clinics. *Journal of Dental Research.* 2020;99:1192–1198.

44. Reardon S. How the Delta variant achieves its ultrafast spread. *Nature, News.* 21 July 2021.

45. Buonanno G, Stabile L, Morawska L. Estimation of airborne viral emission: Quanta emission rate of SARS-CoV-2 for infection risk assessment. *Environment International.* 2020;141(105794).

46. Riediker M, Tsai DH. Estimation of Viral Aerosol Emissions From Simulated Individuals With Asymptomatic to Moderate Coronavirus Disease 2019. *JAMA Network Open.* 2020;3(7):e2013807-e2013807.

47. Sun S, Li J, Han J. How human thermal plume influences near-human transport of respiratory droplets and airborne particles: a review. *Environmental Chemistry Letters.* 2021;19:1971-1982.

Appendix - Model Validation

Experimental data from Yin et. al [33] was used to validate the model-predicted airflow, temperature, and contaminant concentration fields. Shown in Figure 17(a), this single-patient hospital room consisted of an inlet diffuser, a main and an auxiliary outlet, and several distributed heat sources (e.g., occupants, medical equipment, and a TV). A 1% SF_6 tracer-gas mixture was released at a constant low flow-rate of 1 L/hr from a circular sponge. Momentum from coughing, speaking, or breathing was not considered. Vertical profiles of the temperature and velocity fields were measured using eight poles distributed throughout the room, while the profiles of the steady-state tracer-gas concentration were measured at five locations; all are shown in Figure 17(b). For more information on the experimental setup, refer to [33].

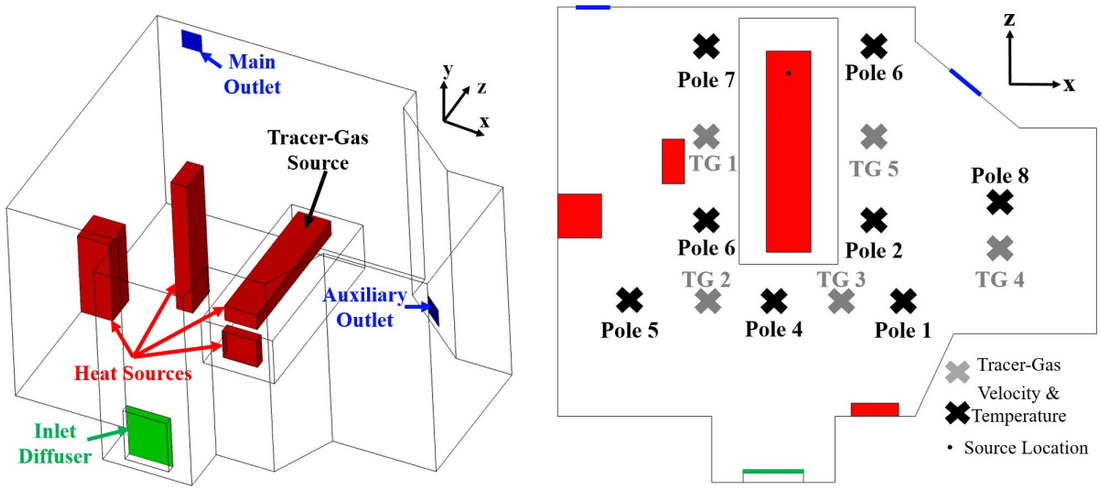

(a) Boundary Conditions (b) Measurement Locations

Figure 17: Description of Yin et al. [33] experimental geometry and measuring locations used to validate the tracer-gas CFD model including (a) the major boundary conditions, and (b) the locations where vertical profiles of the tracer-gas concentration (grey) as well as temperature and velocity (black) were measured at six to eight points spaced vertically in the room.

To show that our model would produce mesh-independent solutions, we ran this validation case with three different unstructured poly-hexcore meshes: a fine, medium, and coarse mesh having maximum cell lengths of 25, 50, and 75 mm with a total number of 3.3, 1.2, and 0.80 million cells, respectively. Each mesh used three surface boundary layer cells on all walls, avoided 1:8 transitions in the octree hex-mesh, and had varying levels of surface refinements for inlets, outlets, and heat sources. Figure 18 shows that all three of these meshes were able to resolve the major features of temperature, velocity, and tracer-gas contaminant concentration fields observed in the experimental data with sufficient accuracy throughout the room. Based on these results, we used the coarse mesh settings, with added refinements near the occupants breath-zones and the PACs, to produce 2.9M and 4.0M cell meshes for the socially-distanced and fully-occupied geometries, described in the Section 3.4.

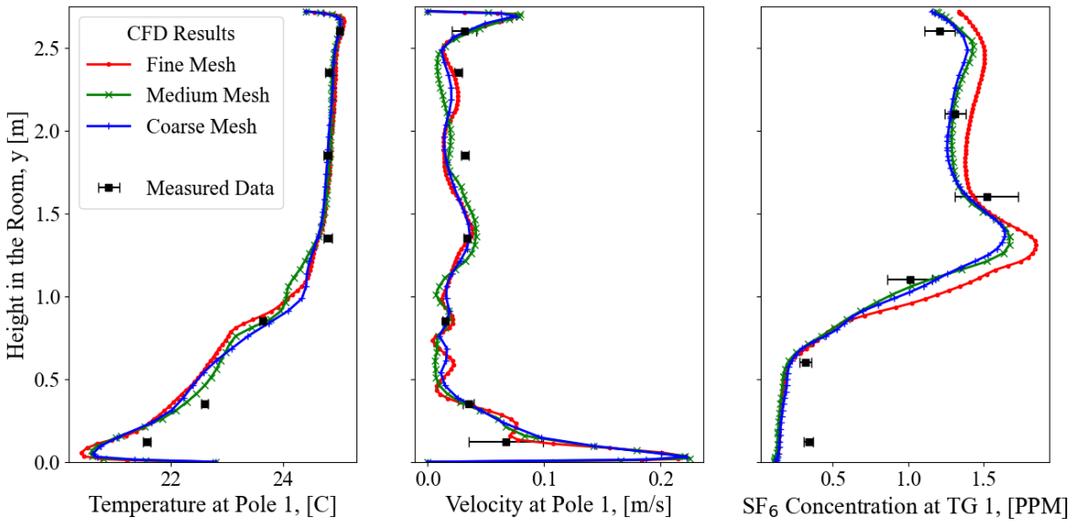

Figure 18: Sample of validation results for the fine (blue), medium (green), and coarse (red) meshed CFD results compared to experimental measurements (black) of the (a) temperature, (b) velocity, and (c) contaminant concentration monitored at different locations throughout the room.